Mean-field theory of the DNLS equation at positive and negative absolute temperatures

OPEN ACCESS

Journal of Statistical Mechanics: Theory and Experiment
An IOP and SISSA journal

PAPER: Classical statistical mechanics, equilibrium and non-equilibrium

Mean-field theory of the DNLS equation at positive and negative absolute temperatures

Michele Giusfredi[1,2,3,*], **Stefano Iubini**[2,3], **Antonio Politi**[2,4] **and Paolo Politi**[2,3]

[1] Dipartimento di Fisica e Astronomia, Università di Firenze, via G. Sansone 1, I-50019 Sesto Fiorentino, Italy
[2] Istituto dei Sistemi Complessi, Consiglio Nazionale delle Ricerche, via Madonna del Piano 10, I-50019 Sesto Fiorentino, Italy
[3] Istituto Nazionale di Fisica Nucleare, Sezione di Firenze, via G. Sansone 1, I-50019 Sesto Fiorentino, Italy
[4] Institute for Complex Systems and Mathematical Biology University of Aberdeen, Aberdeen AB24 3UE, United Kingdom
E-mail: michele.giusfredi@unifi.it, stefano.iubini@cnr.it, a.politi@abdn.ac.uk and paolo.politi@cnr.it

Received 5 February 2026
Accepted for publication 14 April 2026
Published 7 May 2026

Online at stacks.iop.org/JSTAT/2026/053201
https://doi.org/10.1088/1742-5468/ae625e

Abstract. The discrete nonlinear Schrödinger (DNLS) model, owing to the existence of two conserved quantities, exhibits an equilibrium transition from a homogeneous phase at positive absolute temperature to a localized phase at negative absolute temperature. Here, we provide a mean-field (MF) theory of DNLS through a suitable approximation of the grand canonical partition function, which makes it factorizable and can be used to describe the equilibrium state at positive temperatures and the metastable state at negative temperatures. Comparison of our MF results with numerically exact calculations shows that

*Author to whom any correspondence should be addressed.

this approximation is good to excellent in the entire grand canonical phase diagram. Explicit approximate expressions for equilibrium observables are provided in the high-temperature limit. Our theory represents a clear advancement over the model that neglects the interaction between sites.

Keywords: negative temperature, mean-field theory, phase transitions

Contents

1. Introduction

The discrete nonlinear Schrödinger (DNLS) equation is around 50 years old, but it continues to attract the interest of researchers [1–5] for at least two reasons. On the one hand, it has applications in a variety of different fields, ranging from the foundations of statistical mechanics [6] to solid-state physics [7]. On the other hand, its nonlinear and non-integrable character is the basis of interesting nontrivial properties: from a dynamical point of view, the existence of localized breathers [8], and from a statistical point of view, the presence of a negative-temperature (T) regime [9] in a large part of its phase diagram. The two properties are strictly related because the negative-T phase is characterized by the spontaneous emergence of breathers, which are, in principle, metastable [10] (the 'equilibrium' state corresponds to a single breather sitting on top of an infinite-temperature background [11]). However, the rising of breathers is an extremely slow process: for large and negative temperatures, a high barrier hinders their divergence [12]. Moreover, the dynamics itself is extremely slow [13] because of the spontaneous appearance of an adiabatic invariant [14]. As a result, the asymptotic state

J. Stat. Mech. (2026) 053201

may be effectively unachievable [11], making the study of the homogeneous metastable state of special interest.

According to Machlup's criterion, the existence of a negative-T phase is a general property of statistical systems displaying a finite energy density at infinite temperature [15]. In the DNLS case, this occurs because of the existence of two conserved quantities bounded from below: the energy and the mass (or norm). The thermodynamics of DNLS was studied by Rasmussen *et al* [16] in the grand canonical ensemble through the transfer integral operator. This approach allowed to identify an infinite-temperature line of finite energy densities separating homogeneous states at positive temperature from localized negative-T states. In the positive-T region, the formal expression of the grand canonical partition function is usually of unwieldy usage for practical purposes, whereas for negative temperatures it is formally ill-defined because of the divergence of the integral over the grand canonical distribution. This scenario motivated further studies of simplified models sharing some basic features with the full DNLS equation.

A dozen years ago, a purely stochastic model was introduced [9, 17–19], recently renamed the C2C model because it displays a condensed phase induced by two conservation laws. In fact, it shares with the DNLS the existence of two conserved quantities bounded from below: the energy and the mass. The absence of interaction energy between neighboring sites in the C2C model makes it possible to derive some rigorous results [20, 21]. Furthermore, it helped establish a connection with a wider class of stochastic models [22, 23]—the so-called zero-range processes [24]. The C2C model gives an accurate thermodynamical description of the DNLS in proximity of the transition line between homogeneous and localized/condensed phase ($T=\infty$), but it fails when one moves away from this line because C2C disregards the coupling between different sites.

More recently, the DNLS model was studied through a type of mean-field (MF) approach in the large connectivity limit, in which each site interacts with all the others [3]. Another approach has recently used transfer integral techniques to develop an equilibrium description in terms of interacting Rayleigh–Jeans modes beyond the weakly nonlinear limit [5].

In this paper, we introduce an MF description of the DNLS, in which the MF approximation is applied exclusively to the mass variables while treating the phases exactly and keeping nearest-neighbor interactions. The approximation is based on a tweak of the interaction term; we replace the product of variables $x_n x_{n+1}$ on neighboring sites, with the product of the variables on a given site with its statistical average along the system, $x_n\langle x_n\rangle$. As a result, the grand canonical partition function can be factorized, thereby obtaining explicit formulas and reaching a better comprehension of some properties of the DNLS model.

As we are going to see, this allows us to obtain a consistent and semiquantitatively correct description of the whole phase diagram, including the $T=0$ curve and the (metastable) negative-T region. In fact, as shown in [22, 23], the equilibrium state of DNLS at negative T cannot be described in the grand canonical ensemble, but at small negative T it is possible to give a consistent description of the metastable state, which is stable on very long timescales. Therefore, our MF approximation is not only

J. Stat. Mech. (2026) 053201

asymptotically exact in proximity of the transition line, but it also allows obtaining explicit analytical expressions that are applicable on both sides of the critical line.

In section 2, we present the model and the method. The main results of the MF approximation are discussed, distinguishing between positive (section 3) and negative (section 4) temperatures, because in the latter case it is necessary to introduce a cutoff in the mass integral, which defines the partition function. All details of the calculation and the simulations are deferred to the appendices.

2. The model and its MF theory

We start by defining the DNLS model and recalling the most important properties of its phase diagram. In one dimension, the Hamiltonian is

$$H = \sum_n \left[|z_n|^4 + 2J \left(z_n z_{n+1}^* + z_n^* z_{n+1} \right) \right] \tag{1}$$

where z_n is a complex variable describing the state of the system in the site n, and the parameter $J \geqslant 0$ modulates the hopping energy[5]. The corresponding Hamilton's equations are

$$i\dot{z}_n = -2|z_n|^2 z_n - J\left(z_{n-1} + z_{n+1}\right). \tag{2}$$

In this paper, it is convenient to express the equations in terms of action–angle variables, defining $z_n = \sqrt{c_n} e^{i\phi_n}$, where $c_n \geqslant 0$ can be interpreted as a local mass. The Hamiltonian becomes

$$H = \sum_n \left[c_n^2 + 2J\sqrt{c_n c_{n+1}} \cos\left(\phi_n - \phi_{n+1}\right) \right] \equiv N\left(h_{\mathrm{nl}} + h_{\mathrm{int}}\right) = Nh, \tag{3}$$

where h_{nl}, h_{int}, and h are the nonlinear, interaction, and total energy densities, respectively. Consistently, the dynamical equations are $\dot{c}_n = -\partial H/\partial\phi_n$ and $\dot{\phi}_n = \partial H/\partial c_n$. The mass

$$A = \sum_n c_n \equiv Na, \tag{4}$$

as well as the energy, is conserved.

The ground state is characterized by uniform masses ($c_n = a$) and alternating phases ($\phi_{n+1} = \phi_n + \pi$). The ground-state energy is therefore

$$h_{\mathrm{GS}} = a^2 - 2Ja. \tag{5}$$

[5] Negative values of J can be mapped to positive ones via the gauge transformation $\phi_n \to \phi_n + \pi n$ [1].

J. Stat. Mech. (2026) 053201

The transition line between positive and negative temperatures is characterized by an exponential distribution of masses and a random distribution of phases, which implies

$$h_{\mathrm{c}} = 2a^2. \tag{6}$$

The negative-T region appears above the critical line. Its properties are not yet fully understood [12, 18, 22]; they depend on the size of the system, the statistical ensemble describing it, and the timescales over which we observe the system, because the homogeneous phase is actually metastable above the critical line.

In the limit case $J = 0$, the interaction energy h_{int} vanishes, and the angles do not obviously contribute. This corresponds to the so-called C2C model; given the absence of interactions, an evolution can be implemented via a local stochastic dynamical rule that ensures conservation of both mass and energy [17].

Within the grand canonical formalism, the equilibrium properties of the DNLS model can be extracted from the partition function

$$Z(\beta,\mu) = \int_0^\infty \prod_n \mathrm{d}c_n \int_0^{2\pi} \prod_n \mathrm{d}\phi_n \mathrm{e}^{-\beta(H+\mu A)}, \tag{7}$$

where β is the inverse temperature, μ is the chemical potential, and the energy H and mass A are given by equations (3) and (4). The function was evaluated in [16], determining the leading eigenfunction of a suitable transfer integral operator. However, the final expressions are not very handy for the extraction of useful information. Altogether, the main obstacle is that for $J \neq 0$, the interaction energy prevents a factorization of the integrals.

Here, we show that a suitable MF approximation restores the factorization. Our method consists of rewriting the product of masses appearing in the neighboring-site coupling term (see equation (3)) as

$$\sqrt{c_n c_{n+1}} \simeq q\sqrt{c_n}, \tag{8}$$

where $q \equiv \langle\sqrt{c_n}\rangle$ is a statistical average to be determined autoconsistently with Z. Within this approximation, the Hamiltonian H is rewritten as

$$H_{\mathrm{MF}} = \sum_n \left[c_n^2 + 2qJ\sqrt{c_n}\cos\left(\phi_n - \phi_{n+1}\right)\right] \tag{9}$$

and the partition function becomes the product of single-site terms, $Z_{\mathrm{MF}} = z^N$, with

$$z(\beta,\mu) = \int_0^\infty \mathrm{d}c \int_0^{2\pi} \mathrm{d}\varphi\, \mathrm{e}^{-\beta\left(c^2+2qJ\sqrt{c}\cos\varphi\right)+mc}, \tag{10}$$

where φ is the phase difference between neighboring sites, and $m \equiv \beta\mu$.

The integral over the angle φ can be easily calculated, introducing the zero-order modified Bessel function,

$$z(\beta,\mu) = 2\pi \int_0^\infty \mathrm{d}c \exp\left(-\beta c^2 + mc\right) I_0\left(2\beta q J\sqrt{c}\right), \tag{11}$$

where q, as anticipated, must be determined autoconsistently through the relation

$$q \equiv \langle\sqrt{c}\rangle = \frac{2\pi}{z} \int_0^\infty \mathrm{d}c\sqrt{c}\exp\left(-\beta c^2 + mc\right) I_0\left(2\beta q J\sqrt{c}\right). \tag{12}$$

Similar expressions can also be derived for the mass density $a = \langle c\rangle$ and the energy densities $h_{\mathrm{nl}} = \langle c^2\rangle$ and $h_{\mathrm{int}} = \langle 2qJ\sqrt{c}\cos\varphi\rangle$. Without loss of generality, we will assume $J = 1$, because J can be scaled out so long as it is strictly larger than 0.

If $\beta > 0$, the convergence of the integrals appearing in the definition of the various observables is ensured, whereas for $\beta < 0$ the integrand diverges at large c, signaling the well-known instability arising from the appearance of large peaks (breathers). For this reason, negative temperatures require a special treatment, and we have devoted an entire section to their discussion. In brief, although negative-temperature localized states in the DNLS model are formally well-defined only in the microcanonical ensemble [4, 22, 23], homogeneous metastable states have been recently shown to admit a consistent description in terms of a regularized grand canonical theory [12]. In this paper, we will restrict ourselves to this class of negative-temperature states.

Independently of the sign of β, it is convenient to introduce the smallness parameter $w = 1/(\beta\mu^2) = \beta/m^2$ ($m = \beta\mu \to -1/a$ for $\beta \to 0$), which allows the derivation of simple and accurate formulas in the small $|\beta|$ region (see appendix B for the derivation of the expressions for the most relevant observables).

For instance, at leading order in w, the following expressions hold across the critical line, i.e. for both positive and negative temperatures:

$$q = \frac{\sqrt{\pi}}{2\sqrt{|m|}} - \frac{7\sqrt{\pi}\,w}{8\sqrt{|m|}} + O\left(w^2\right) \tag{13}$$

$$a = \frac{1}{|m|} - \frac{4w}{|m|} + O\left(w^2\right) \tag{14}$$

$$h_{\mathrm{nl}} = \frac{2}{m^2} - \frac{20w}{m^2} + O\left(w^2\right) \tag{15}$$

$$h_{\mathrm{int}} = -\frac{\pi}{2}w + O\left(w^2\right). \tag{16}$$

3. Positive temperatures

In the positive-T regime, the equilibrium state can be equivalently described by the microcanonical and grand canonical ensembles [22, 23]. Within the MF approximation,

J. Stat. Mech. (2026) 053201

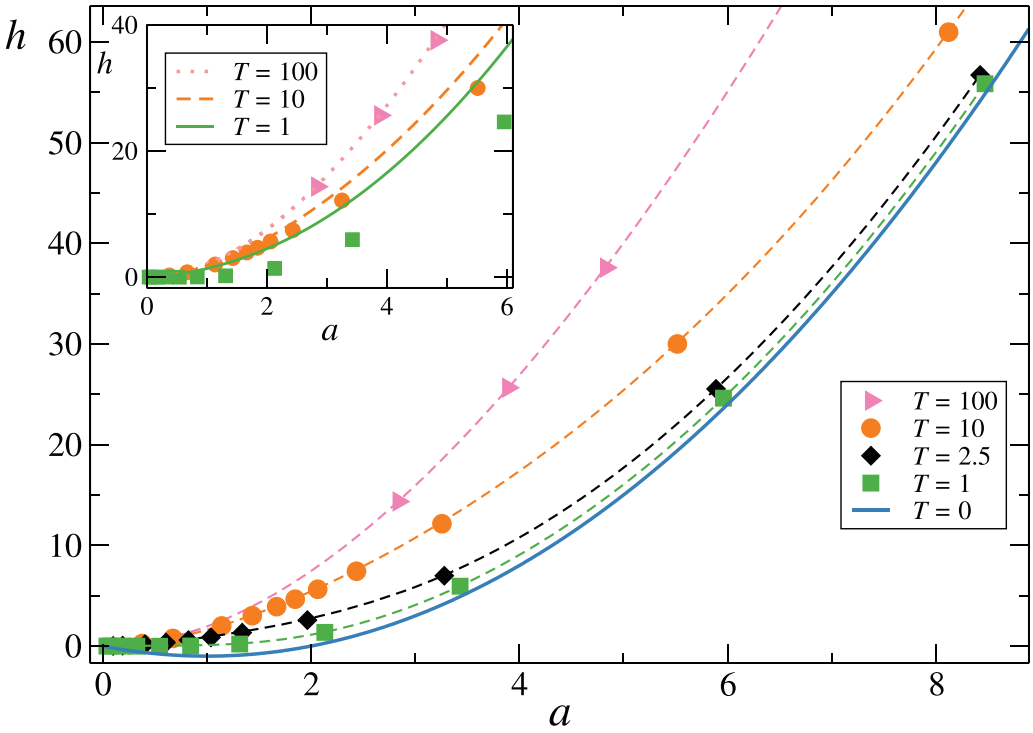

Figure 1. Main: comparison between the MF theory (curves) and the exact results obtained via grand canonical simulations (symbols). Each curve corresponds to a different $T = 1/\beta$, decreasing from top to bottom according to the legends. At $T = 0$, the ground-state curves for DNLS and its MF approximation are known exactly, and they coincide (full line). Inset: comparison between the C2C model (curves) and the exact results (symbols). The agreement is acceptable only for very large T. The size of the system is $N = 100$, and details about the simulations are given in appendix A.

this means that the single-site partition function (see equation (10)) is well defined and finite for any $\beta \geqslant 0$ and for any m (i.e. for any μ).

In figure 1, we compare the virtually exact results obtained via grand canonical simulations (symbols) with MF curves (main panel) and with the C2C model (inset) (see appendix A for numerical details). These data show that the isothermal curves $h(a)$ are exceptionally well reproduced by the MF theory, down to $T = 0$. In fact, the ground-state energy has the same analytical expression, $h_{\mathrm{GS}}(a) = h^2 - 2Ja$. The agreement is not as good for the C2C model, as shown in the inset of the same figure; already at $T = 10$, the isothermal curve of C2C compares very poorly with exact results.

In figure 2, the validity of the MF theory is also tested in the planes (a, μ) and (h, μ). There, the agreement with the numerical data is very good at high T, whereas it worsens with decreasing T. Remarkably, it appears that the deviation essentially amounts to a shift of the chemical potential by one unit, as it can be appreciated by looking at the dashed curve, which corresponds to $\mu - 1$. As shown in appendix C, the shift is a rigorous property at zero temperature, and it is essentially irrelevant while

J. Stat. Mech. (2026) 053201

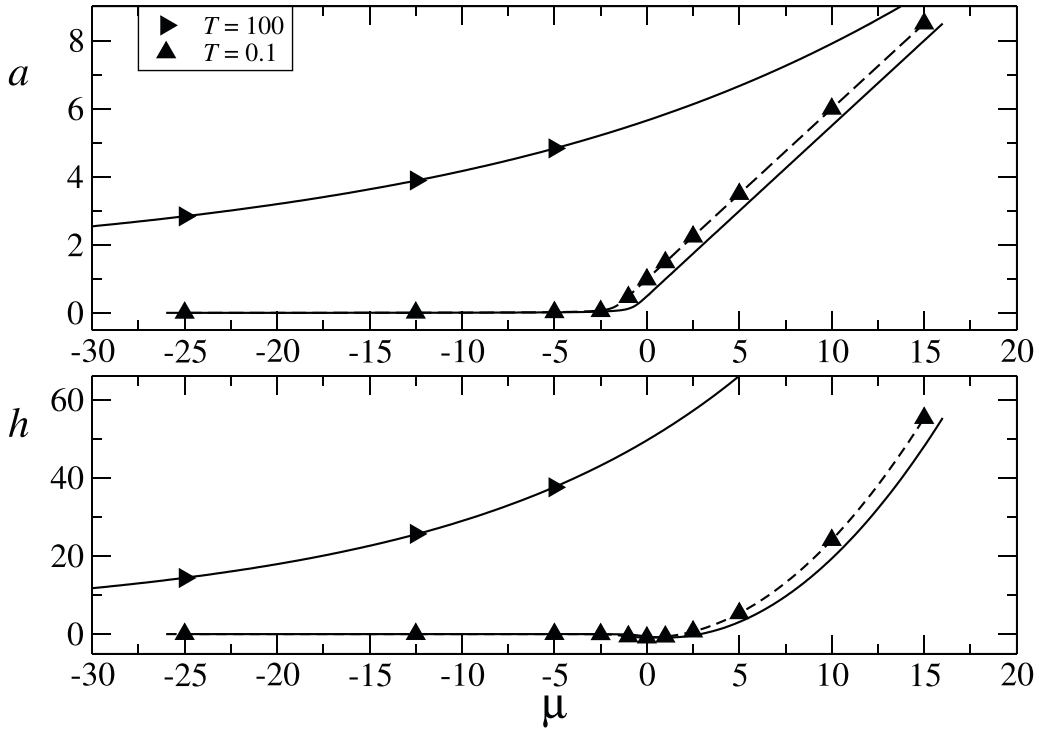

Figure 2. Same as in figure 1 main, but we now compare MF and exact numerical results in the planes (μ, a) and (μ, h) rather than in (a, h). In this way, a horizontal shift at low temperature is evident, arising from an incorrect determination of the chemical potential in the MF theory. Symbols: exact results from grand canonical simulations. Full lines: MF approximation. Dashed lines: MF approximation corrected for the chemical potential: $\mu \to \mu - 1$.

approaching the transition line for finite a, as μ diverges therein, so that the curves for μ and $\mu - 1$ practically coincide.

We now discuss the relative role of $h_{\rm nl}$ and $h_{\rm int}$ for a double reason: (1) because it allows a further test of the MF approximation, and (2) because it is an aspect of DNLS that has been little considered in its studies. From the literature, we know only that $h_{\rm int}$ vanishes on the critical line, which is the reason why the C2C model is statistically equivalent to DNLS in its proximity. Below, we try to understand more quantitatively how the energy is distributed between the two terms, both in the exact DNLS theory and in its MF approximation.

In figure 3, we present the dependence of $h_{\rm nl}$ and $h_{\rm int}$ versus the total energy h for two values of the mass density. To facilitate the comparison, the total energy is suitably shifted and scaled in such a way that the zero of the horizontal axis corresponds to $T = 0$, whereas 1 corresponds to infinite temperature. This corresponds to plot $x = (h - h_{\rm GS})/(h_{\rm c} - h_{\rm GS})$. Similarly, the two energy terms are scaled by the critical energy; therefore, we plot $y_{\rm nl,int} = h_{\rm nl,int}/h_{\rm c}$. Using the new variables, we have $y_{\rm nl}(0) = \frac{1}{2}$ and $y_{\rm nl}(1) = 1$, whereas $y_{\rm int}(0) = -1/a$ and $y_{\rm int}(1) = 0$. We stress that the MF results (lines)

J. Stat. Mech. (2026) 053201

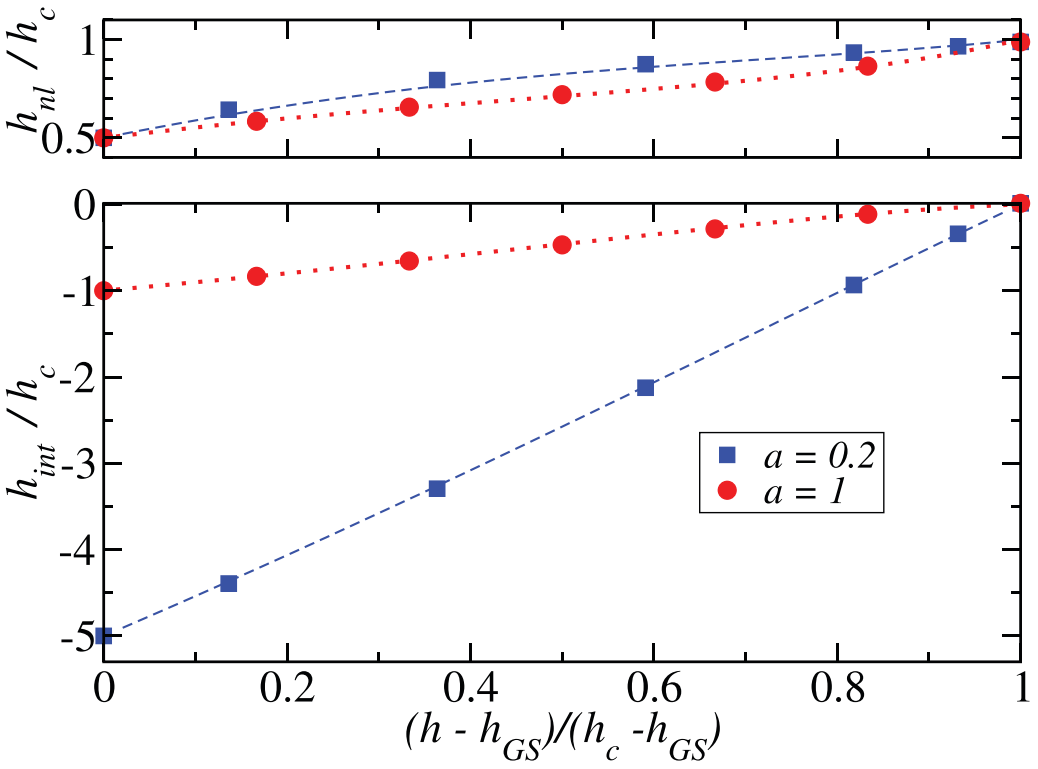

Figure 3. Relative contributions $h_{\rm int}$ (lower panel) and $h_{\rm nl}$ (upper panel) are presented versus the total energy h suitably rescaled (see the main text). Symbols are the exact results from the microcanonical simulations, as described in appendix A. Dashed ($a = 0.2$) and dotted ($a = 1$) lines are the MF results.

compare very well with the exact results (symbols). It is also remarkable that both functions $y_{\rm nl,int}(x)$ are close to linear.

It is not possible to derive analytically the behavior of $y_{\rm nl,int}(x)$ within the MF theory, because this theory works with the grand canonical variables β, μ, and their relations with a and h can be obtained numerically, with no closed-form solutions available. However, we can use the expansions in w, which is what we are going to do now. For this purpose, we have identified a quantity that, for small w, depends on a single parameter, namely m (see appendix D),

$$R = \frac{h_{\rm c} - h_{\rm nl}}{h_{\rm c} - h} \,. \tag{17}$$

This is the ratio between the distance of the nonlinear energy from the $\beta = 0$ value (for the same mass density) and the distance of the full energy, again from the $\beta = 0$ value.

In the positive-temperature region, both the numerator and the denominator defining R are positive. Moreover, since $h_{\rm int} \leqslant 0$, the numerator is smaller than the denominator so that $0 \leqslant R \leqslant 1$. However, it is not straightforward to identify the locations in parameter space where the limit values can be achieved. In fact, for R being equal to 1, it is necessary that $h_{\rm int} = 0$, which occurs when the denominator and the numerator

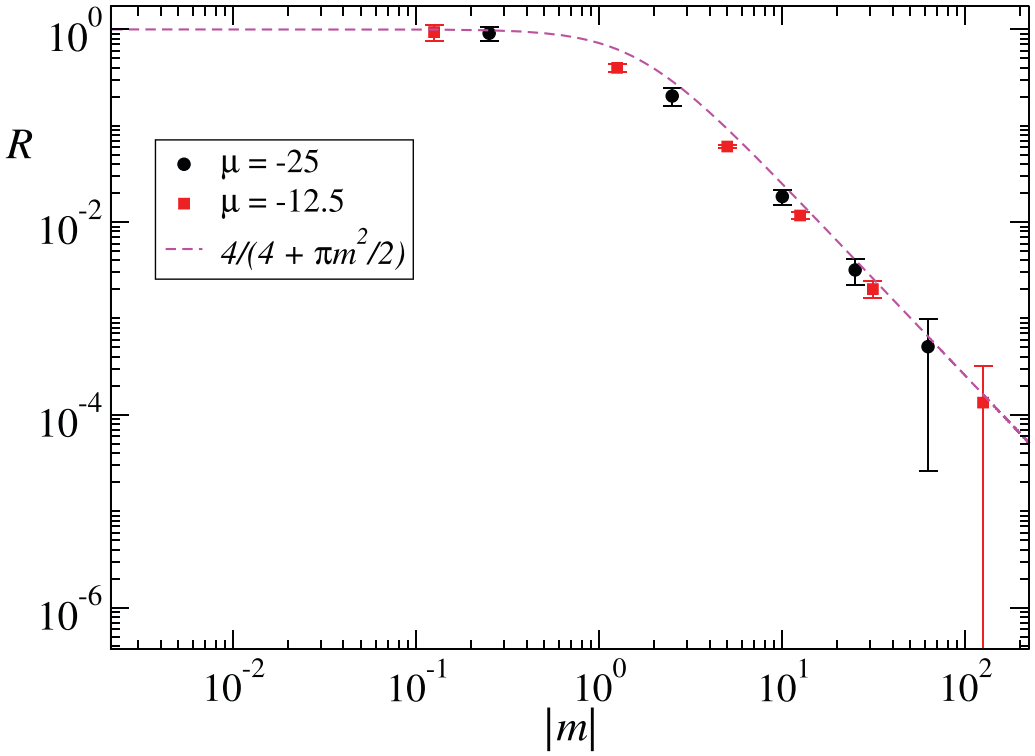

Figure 4. Dependence of the parameter $R = (h_c - h_{nl})/(h_c - h)$ versus $|m|$. Symbols refer to the numerical simulation of the full DNLS model, whereas the dashed line refers to the analytical prediction of the MF theory.

are both equal to 0. Furthermore, $R = 0$ requires $h_{nl} = 2a^2$, which again occurs when the denominator vanishes.

MF analysis helps to clarify the issue, as shown in figure 4, where we plot R for different values of μ and β, comparing numerical results for the full DNLS model (symbols) with the analytical curve $R = 4/(4 + \pi m^2/2)$, found within the MF approximation, in a $w-$expansion. At the lowest order in w, R is a function only of m, not of w. It is worth recalling that $m = \beta\mu$ is equal to $-1/a$ on the critical curve $\beta = 0$. On the other hand, if we fix μ and vary β, the limit of small β corresponds to small m. Let us start from this limit, because for $\beta \to 0$, $h_{nl} \to 0$ and $R \to 1$; this is what we observed in figure 4. We can also monitor the regime $|m| \ll 1$, provided that w is small. On the critical curve, this simply implies $a \ll 1$, and in this limit $R \simeq a^2$, which means that for small mass density a, when h approaches h_c, h_{nl} is practically on the critical curve.

It is worth stressing that the approximation $R = 4/(4 + \pi m^2/2)$ is not valid for vanishing T. In this limit, m diverges, which would imply a vanishing R, whereas in reality R goes to a constant:

$$\lim_{T \to 0} R = \frac{a^2}{a^2 + 2a}. \tag{18}$$

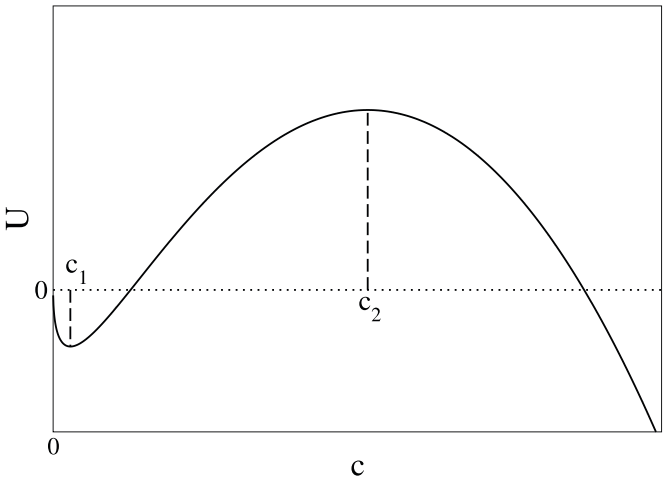

Figure 5. Sketch of the potential $U(c)$, equation (20), for $\phi = 0$ and small negative β.

4. Negative-temperature homogeneous states

States with energy density above the critical line $h_c(a)$ display negative temperatures and are expected to develop a thermodynamic instability, resulting in the condensation of a macroscopic peak [16]. The theoretical description of this mechanism requires a microcanonical formalism, whereas the grand canonical measure is formally ill-defined [22, 23]. Previously, it was shown that homogeneous states slightly above the critical line (i.e. with $|\beta| \ll 1$) are metastable, in the sense that the characteristic time to develop the localization instability grows exponentially with $|T|$ [12]. In this regime, an effective grand canonical description can be developed in terms of an asymptotically unstable thermodynamic potential with a metastable region for low-amplitude states. The fundamental properties of the effective potential were derived in [12] under the approximation that the hopping term of the DNLS Hamiltonian is negligible with respect to the nonlinear one, thereby removing any explicit phase dependence. In the following, we generalize this derivation to include phases within the MF approximation.

For $\beta < 0$, we introduce a cutoff c^* with value that is univocally determined by the potential (see below). Having established this, equation (10) is modified as follows:

$$z(\beta, m) = \int_0^{c^*} \mathrm{d}c \int_0^{2\pi} \mathrm{d}\phi \exp\left[-U(c, \phi; \beta, m)\right], \tag{19}$$

where we have rewritten the exponent as a two-dimensional potential having the form

$$U(c, \phi; \beta, m) = \beta c^2 + 2\beta q \sqrt{c} \cos\phi - mc. \tag{20}$$

Notice that the parameters β and m are both negative, thereby yielding a potential (20), the shape of which is qualitatively plotted in figure 5 for $\phi = 0$.

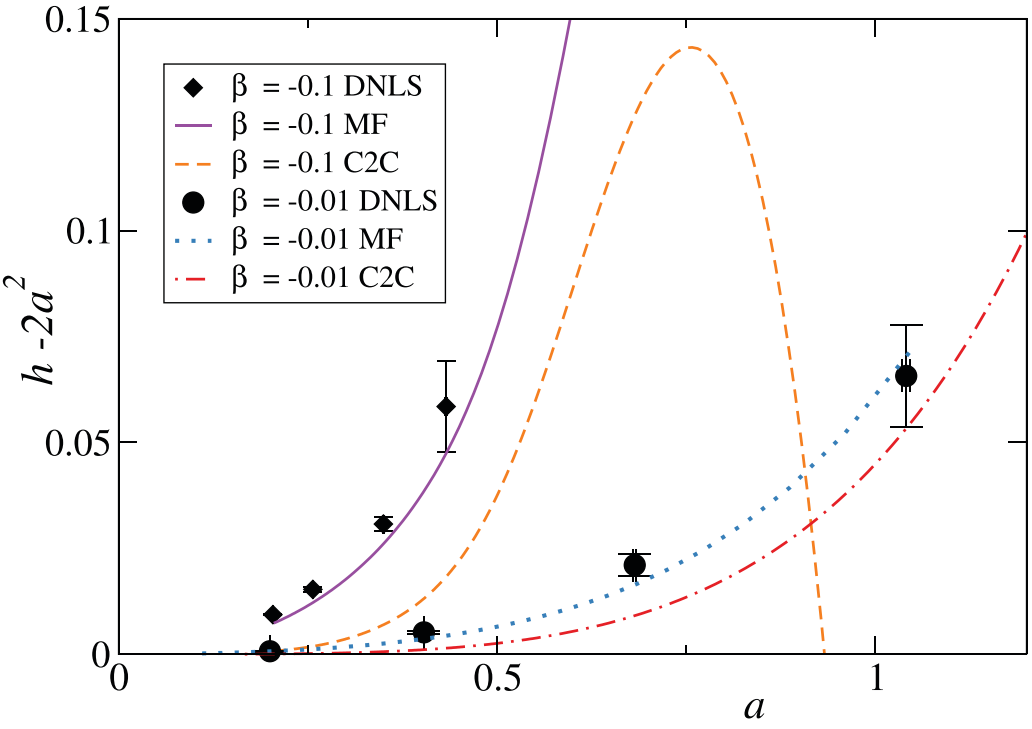

Figure 6. Comparison of exact numerical results (symbols) with MF predictions (full and dotted lines) and with the C2C model (dashed and dotted–dashed lines). We performed this comparison for two negative temperatures: $\beta = -0.1$ and $\beta = -0.01$. It is evident that we are in the negative-T region because $(h - 2a^2) > 0$. We also indicate the statistical error bar for the symbols, obtained as spatial and temporal averages of grand canonical simulations.

The theory of the metastable state proceeds as follows. We begin by determining the lowest barrier, corresponding to $\phi = 0$. This barrier (which is a function of q) determines z and any thermodynamic average, including $q = \langle\sqrt{c}\rangle$ itself. Once q has been found self-consistently, we have a theory that allows us to pass from the grand canonical variables β, μ to the microcanonical variables a, h. In the C2C model [12], the procedure is similar but easier because $c^* = m/2\beta$ is independent of q.

In figure 6, we compare virtually exact numerical results for the DNLS model with its MF approximation and with results for the C2C model (see the legend for more details). Simulations of the DNLS equations have been performed using negative-temperature Monte Carlo (grand canonical) reservoirs (see appendix A). We performed this analysis in the plane $(h - 2a^2, a)$ to better highlight the small differences between the energy and the critical energy. Although the MF theory gives a relatively accurate approximation, the C2C model does not, even for the smallest (negative) inverse temperature, $\beta = -0.01$. For $\beta = -0.1$, the C2C model not only compares poorly with DNLS but also displays a reentrant behavior.

This is because, for larger a, the confining character of the potential is restricted to a progressively smaller interval of negative β, and the stability of the homogeneous state is quickly lost. Outside this condition, it is therefore no longer possible to give

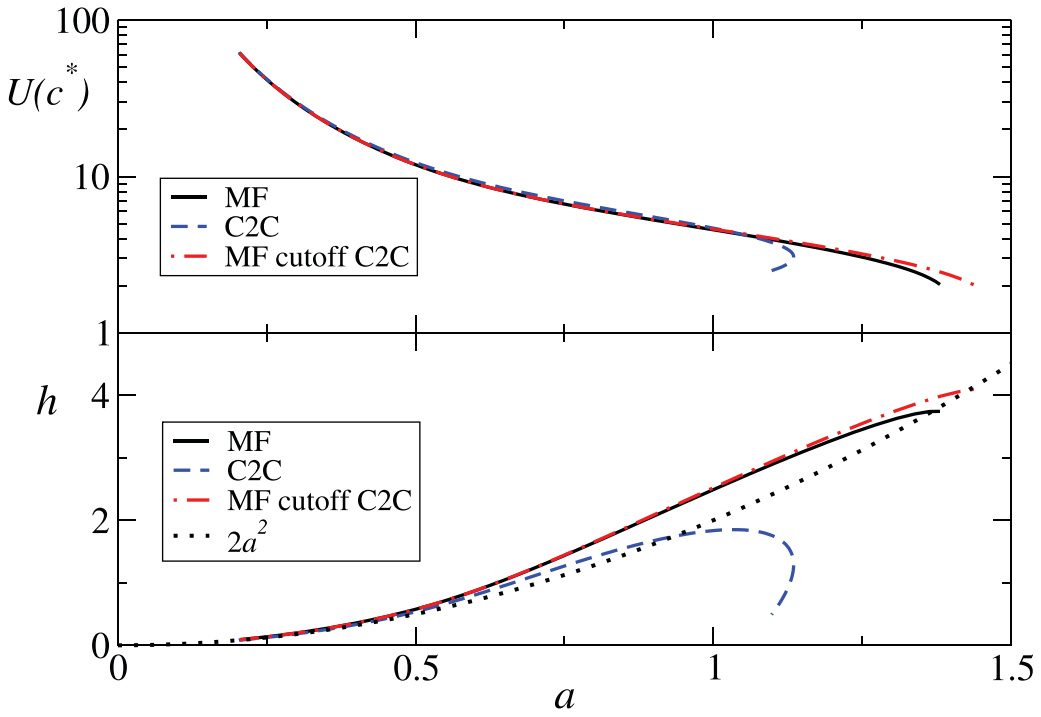

Figure 7. Top: comparison of the height of the barrier for the MF theory, the C2C model, and the MF theory using the C2C cutoff. Bottom: the same type of comparison, for the parametric curves $h(a)$. The data refer to $\beta = -0.1$ and variable μ in the interval $(10, 50)$.

a grand canonical description. An inspection of potential (20) allows us to be more precise, distinguishing among small, intermediate, and large c values $U(c) \approx -\sqrt{c}, c, -c^2$, respectively.

The crossover from the first to the second regime occurs at $c_1 \simeq \beta^2 q^2/m^2$, whereas the crossover from the second to the third regime occurs at $c_2 \simeq |m/\beta|$. For the potential to be partially confining, it is therefore necessary that c_2 is sufficiently larger than c_1. This implies $|m| \gg |\beta| q^{2/3}$, which, in the limit of small β, leads to $a \ll 1/|\beta|^{3/4}$. This is a necessary condition to have some confinement; the condition to have stability on a meaningful timescale is much stronger, but it is not possible to make predictions without studying the dynamics.

The fact that the MF theory provides a better description of DNLS than the C2C model is not because of a better evaluation of the cutoff c^* or of the energy barrier $U(c^*)$; it is because the interaction energy is not entirely negligible. This is shown in figure 7, the upper panel of which compares the height of the barriers for the MF theory, the C2C model, and the MF theory using the C2C cutoff. Up to $a = 1$, the three curves are practically indistinguishable, but this is no longer true in the lower panel, where the corresponding parametric curves are plotted. The curves obtained by using the MF theory with the C2C cutoff have a double purpose: to stress the secondary importance of the cutoff and to justify the approximation made in figure 6, where we used the C2C cutoff to plot the MF results. This trick greatly simplifies the analysis in the MF case.

The reentrant character of the curves in figures 6 and 7 is a consequence of the modest bounding capacity of the potential so that the grand canonical theory is unable to give a correct description of the system. In some sense, it is a 'static' proxy of the loss of metastability.

5. Conclusions

In this study, we have developed an MF approach and thereby derived a grand canonical description of the DNLS model. This includes the equilibrium state at any positive temperature and the homogeneous metastable state emerging at large negative temperatures. The approximation involves assuming that the interaction term is gauged by the average mass (amplitude) of the neighboring sites rather than by their actual values. This approximation has no effect on either the critical curve (because the interaction term is negligible) or the ground-state curve (because all masses are equal). On the other hand, it is crucial for the phases to be handled accurately, which this approximation ensures. Therefore, the MF approximation is a step forward compared to the stochastic C2C model, in which the coupling term is completely neglected and phase variables do not appear.

Our results show that the MF approximation provides a good-to-excellent description of the system for all values of mass and energy densities via a direct grand canonical description. In particular, it provides an accurate characterization across the transition from positive to negative temperature, where instabilities are expected to arise. In fact, although MF theories typically fail in proximity of phase transitions, here the approximation works because the interaction energy is negligible, and the transition itself occurs even in the absence of interactions. Our approach shows that the presence of interactions ensures a smooth crossing of the critical curve. The negative-T equilibrium state cannot be described by the grand canonical theory, but for small negative β, the system is trapped for a long time in a metastable state. This passage is smooth, and equations (13)–(16) are equally valid for positive and negative temperatures.

The ensuing transition from the homogeneous metastable state to the localized equilibrium state goes beyond the scope of this study. It would require the formulation of an appropriate dynamical rule consistent with the MF approximation introduced in this paper.

Acknowledgments

SI and PP acknowledge the financial support from the Italian MUR PRIN2022 project 'Breakdown of ergodicity in classical and quantum many-body systems' (BECQuMB) Grant No. 20222BHC9Z.

J. Stat. Mech. (2026) 053201

Appendix A. Technical details of the numerical simulations

The simulations of the full DNLS model were performed on a chain of size $N = 100$ with periodic boundary conditions, interacting with a thermal reservoir at site $n = 1$. The evolution was studied by introducing the conjugate canonical variables

$$v_n = \sqrt{2c_n}\cos\phi_n,\ u_n = \sqrt{2c_n}\sin\phi_n, \quad n = 1,\ldots,N, \tag{A.1}$$

with time dependence that is ruled by the following equations of motion

$$\dot{v}_n = -\left(v_n^2 + u_n^2\right)u_n - u_{n-1} - u_{n+1} \tag{A.2}$$

$$\dot{u}_n = \left(v_n^2 + u_n^2\right)v_n + v_{n-1} + v_{n+1}. \tag{A.3}$$

We implemented this Hamiltonian dynamics using a 4th-order Runge–Kutta algorithm with an integration step $\delta t = 10^{-3}$.

The DNLS chain was thermostatted at temperature $T = \beta^{-1}$ and chemical potential μ with a Monte Carlo heat bath [25]. Once every $t = 1$ units of time, we generated new canonical variables for site 1, $u_1' = u_1 + \delta u_1'$ and $v_1' = v_1 + \delta v_1$, where δu_1 and δv_1 were random variables extracted from the uniform distribution in the interval $[-0.5, 0.5]$. We then updated the canonical variables using a Metropolis algorithm by evaluating the cost function $W = \exp\left(-\beta\Delta E + m\Delta A\right)$, where

$$\Delta A = \frac{u_1'^2 + v_1'^2}{2} - \frac{u_1^2 + v_1^2}{2} = c_1' - c_1 \tag{A.4}$$

$$\Delta E = c_1'^2 - c_1^2 + \left(u_N + u_2\right)\delta u_1 + \left(v_N + v_2\right)\delta v_1 \tag{A.5}$$

are the variations in mass and energy, respectively. When $W > 1$, we updated u_1 and v_1 with u_1' and v_1', whereas when $W < 1$ the move was accepted with probability W. This algorithm was implemented in the same way regardless of the sign of β [6].

The initial conditions were typically selected as 'infinite temperature' configurations, i.e. with phases ϕ_n extracted from the uniform distribution in $[0, 2\pi]$ and masses c_n generated from an exponential distribution $f(c) = 1/a_i \exp(-c/a_i)$, with a_i chosen appropriately for each simulation to be close to the mass density reached at equilibrium.

The values of a, h, and h_{nl} were obtained from a combination of spatial and temporal averages of local quantities. With the canonical variables u_n and v_n, the local masses were $c_n = \frac{1}{2}(u_n^2 + v_n^2)$. We can also define local energies ϵ_n as

$$\epsilon_n \equiv \frac{1}{4}\left(u_n^2 + v_n^2\right)^2 + \frac{1}{2}\left(u_{n-1} + u_{n+1}\right)u_n + \frac{1}{2}\left(v_{n-1} + v_{n+1}\right)v_n, \tag{A.6}$$

which correspond to the sum of the nonlinear local energy c_n^2 and half the coupling energy between sites $n-1$ and n and between n and $n+1$, so that $\sum_{n=1}^{N}\epsilon_n = H$. We first considered, for each site, a time average of c_n, ϵ_n, and c_n^2, from which we obtained spatial averages yielding a, h, and h_{nl}, respectively. Time averages were taken over intervals between 10^7 and 10^8 time units, after waiting for a transient $t = 10^5$. Only the 80 internal sites of the chain contributed to the spatial averages (to remove any effects

J. Stat. Mech. (2026) 053201

arising from the heat bath connected to site 1, with the first and last ten sites in the chain excluded). The uncertainties of the averages were obtained from the standard deviation of the spatial average, and in all figures such uncertainties were either shown or were smaller than the symbol size.

Appendix B. Small-β expansion

In this appendix, we derive the analytical expressions of the MF theory for small β.

Let us start with the case $\beta > 0$. The reduced grand canonical partition function of the MF model, equation (11) ($J = 1$),

$$z = 2\pi \int_0^\infty \mathrm{d}c\, \mathrm{e}^{-\beta c^2 + mc} I_0\left(2\beta q\sqrt{c}\right) \tag{B.1}$$

can be rewritten as

$$z = \int_0^\infty \mathrm{d}c \sum_{n=0}^\infty \mathrm{e}^{\left(-\beta c^2 + mc\right)} \frac{2\pi}{(n!)^2} (\beta q)^{2n} c^n, \tag{B.2}$$

using the Taylor expansion of the modified Bessel function I_0,

$$I_0(v) = \sum_{n=0}^\infty \frac{1}{(n!)^2} \left(\frac{v}{2}\right)^{2n}. \tag{B.3}$$

Because the series in the integrand of equation (B.2) absolutely converges for any positive c, we can swap the order of integration and summation, and then individually integrate the terms of the series, from which we obtain

$$z = \sum_{n=0}^\infty 2^{-n} \beta^{-(1+3n)/2} q^{2n} \pi\, U\left(\frac{1+n}{2}, \frac{1}{2}, \frac{m^2}{4\beta}\right), \tag{B.4}$$

where U is the Tricomi's confluent hypergeometric function.

Similarly, it is possible to obtain the average value of any power α of c as a function of β, m, and q,

$$\begin{aligned}
\langle c^\alpha \rangle &= \frac{1}{z} \int_0^\infty \mathrm{d}c \int_0^{2\pi} \mathrm{d}\varphi\, c^\alpha\, \mathrm{e}^{-\beta c^2 + mc - 2\beta q\sqrt{c}\cos\varphi} \\
&= \frac{2\pi}{z} \int_0^\infty \mathrm{d}c\, c^\alpha\, \mathrm{e}^{-\beta c^2 + mc} I_0\left(2\beta q\sqrt{c}\right) \\
&= \frac{1}{z} \sum_{n=0}^\infty 2^{-n-\alpha} \pi\, \beta^{(n-1-\alpha)} (\beta q)^{2n} \Gamma(n+1+\alpha) \\
&\quad \times U\left(\frac{n+1+\alpha}{2}, \frac{1}{2}, \frac{m^2}{4\beta}\right),
\end{aligned} \tag{B.5}$$

from which we have the expression for the mass density a for $\alpha=1$ and for the nonlinear energy $h_{\rm nl}$ for $\alpha=2$. We can also express the self-consistency relation $q=\langle\sqrt{c}\rangle$ using equation (B.5) with $\alpha=1/2$,

$$q=\langle\sqrt{c}\rangle=\frac{\pi}{z}\sum_{n=0}^{\infty}2^{-n-1/2}\beta^{3n/2-3/4}\frac{q^{2n}}{(n!)^2}\Gamma\left(\frac{3}{2}+n\right)\times U\left(\frac{3}{4}+\frac{n}{2},\frac{1}{2},\frac{m^2}{4\beta}\right) \tag{B.6}$$

For the interaction energy density $h_{\rm int}$, we have instead

$$\begin{aligned}h_{\rm int}&=\frac{1}{z}\int_0^{\infty}{\rm d}c\int_0^{2\pi}{\rm d}\varphi\;2q\sqrt{c}\cos\varphi\,{\rm e}^{-\beta c^2+mc-2\beta q\sqrt{c}\cos\varphi}\\&=-\frac{4\pi q}{z}\int_0^{\infty}{\rm d}c\sqrt{c}{\rm e}^{-\beta c^2+mc}I_1\left(2\beta q\sqrt{c}\right)\\&=\frac{1}{z}\sum_{n=1}^{\infty}\frac{2^{-n}\beta^{-2+3n/2}mq^{2n}}{(n-1)!}U\left(1+\frac{n}{2},\frac{3}{2},\frac{m^2}{4\beta}\right),\end{aligned} \tag{B.7}$$

where we have used the expansion of I_1,

$$I_1(v)=\frac{\rm d}{{\rm d}v}I_0(v)=\sum_{n=1}^{\infty}\frac{n}{(n!)^2}\left(\frac{v}{2}\right)^{2n-1}. \tag{B.8}$$

It is now convenient to introduce the smallness parameter $w=\beta/m^2$, which appears as the argument of the hypergeometric function U. In particular, $U(\cdot,\cdot,1/4w)$ admits an asymptotic expansion for $w\to 0$ in terms of the generalized hypergeometric series ${}_2F_0$ [26],

$$U\left(a,b,\frac{1}{4w}\right)\simeq(4w)^a\,{}_2F_0\left(a,a-b+1;;-4w\right), \tag{B.9}$$

where ${}_2F_0(a,a-b+1;;-4w)$ does not converge in $w=0$ but exists as a formal power series in w.

From now on, we also consider $m<0$. By replacing $\beta=wm^2$ and expanding U in powers of w in equation (B.4), we get

$$z=\frac{2\pi}{|m|}-\frac{4\pi w}{|m|}+\left(\frac{24\pi}{|m|}+2m^2\pi q^2\right)w^2+O\left(w^3\right), \tag{B.10}$$

which we can substitute in equation (B.6) to obtain

$$q=\frac{\sqrt{\pi}}{2\sqrt{|m|}}-\frac{7\sqrt{\pi}}{8\sqrt{|m|}}w+\frac{\sqrt{\pi}\left(449+16|m|^3q^2\right)}{64\sqrt{|m|}}w^2+O\left(w^3,q^4\right). \tag{B.11}$$

The self-consistency relation can therefore be solved in a perturbative way at an arbitrary order of w, from which we obtain

$$q = \frac{\sqrt{\pi}}{2\sqrt{|m|}} - \frac{7\sqrt{\pi}}{8\sqrt{|m|}}w + \frac{449\sqrt{\pi} + 16|m|^2\pi^{3/2}}{64\sqrt{|m|}}w^2 + O\left(w^3\right). \tag{B.12}$$

Once q has been determined, we can replace it into the expressions (B.10), (B.5), and (B.7) to obtain

$$z = \frac{2\pi}{|m|} - \frac{4\pi}{|m|}w + \frac{\pi\left(24 + 2|m|^3q^2\right)}{|m|}w^2 + O\left(w^3\right) \tag{B.13}$$

$$a = \frac{1}{|m|} - \frac{4w}{|m|} + \left(\frac{40}{|m|} + \frac{|m|\pi}{4}\right)w^2 + O\left(w^3\right) \tag{B.14}$$

$$h_{\mathrm{nl}} = \frac{2}{m^2} - \frac{20w}{m^2} + \frac{\left(296 + m^2\pi\right)w^2}{m^2} + O\left(w^3\right) \tag{B.15}$$

$$h_{\mathrm{int}} = -\frac{\pi w}{2} + \frac{15\pi w^2}{4} + O\left(w^3\right) \tag{B.16}$$

$$h = \frac{2}{m^2} - \left(\frac{\pi}{2} + \frac{20}{m^2}\right)w + \left(\frac{19\pi}{4} + \frac{296}{m^2}\right)w^2 + O\left(w^3\right). \tag{B.17}$$

The combination of equations (B.14) and (B.17) gives, for $T = \infty$ (i.e. for $w = 0$),

$$h = 2a^2. \tag{B.18}$$

Let us now consider the case in which $\beta < 0$ and $m < 0$. We can write the reduced partition function z as

$$z = 2\pi \int_0^{\frac{m}{2\beta}} \mathrm{d}c\, \mathrm{e}^{-\beta c^2 + mc} I_0\left(2\beta q\sqrt{c}\right), \tag{B.19}$$

where the cutoff in the mass integration $c^* = \frac{m}{2\beta}$ is the same as that assumed in the study of the C2C model.

If we express β as $\beta = wm^2$ and expand the integrand function in powers of w up to order w^2, we obtain

$$\begin{aligned} z &\simeq 2\pi \int_0^{\frac{m}{2\beta}} \mathrm{d}c\, \mathrm{e}^{mc}\left(1 - c^2m^2w + cm^4\left(\frac{c^3}{2} + q^2\right)w^2\right) \\ z &= \frac{2\pi}{|m|} - \frac{4\pi}{|m|}w + \frac{\pi\left(24 + 2|m|^3q^2\right)}{|m|}w^2 + O\left(w^3\right), \end{aligned} \tag{B.20}$$

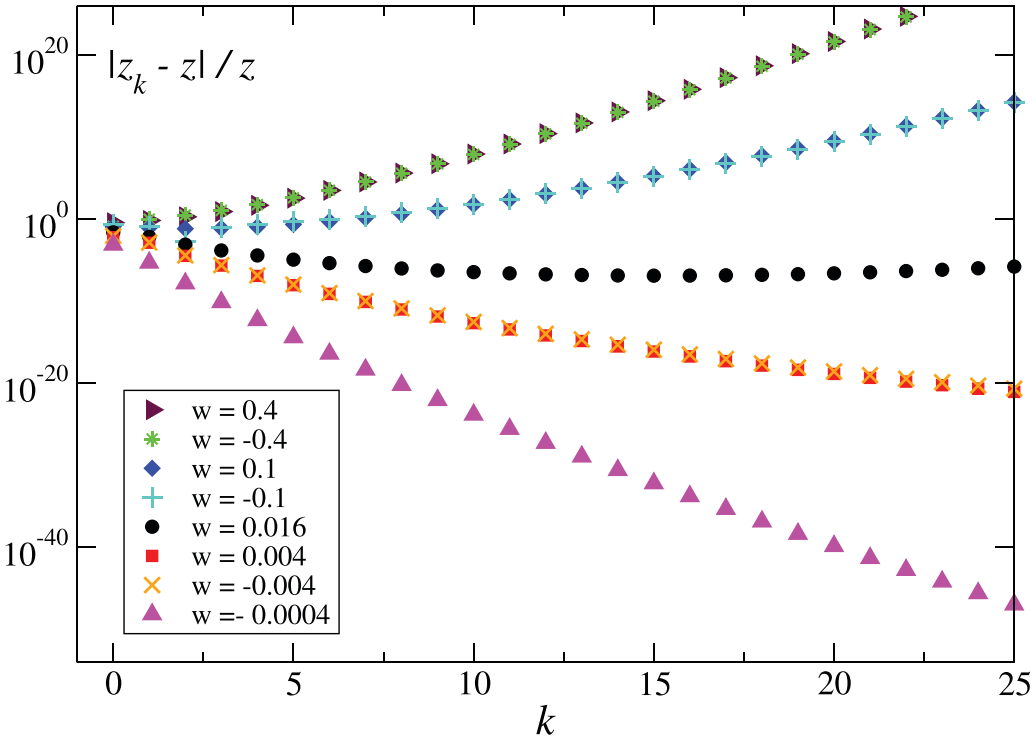

Figure B1. Relative difference between the MF partition function z computed by numerically integrating the exact expression (11) and its analytical approximation z_k, obtained as a series expansion of order k in w. The various symbols correspond to different w values, as indicated in the legend. The value of β is always equal to ± 0.4, except for the lowermost curve, where $\beta = -0.01$. Notice that the sign of β coincides with the sign of w. For negative β, the numerical integration is performed by imposing the same cutoff c^* as in the C2C model.

which is equal to equation (B.10). We therefore find that the expansion of z at negative temperatures coincides with that at $\beta > 0$. An adjustment of the cutoff leads only to corrections of order $\mathrm{e}^{-1/(2|w|)}$.

Similarly, from the calculation of q, a, h_{nl}, and h_{int}, we find that the expressions (B.12)–(B.17) are also valid for $\beta < 0$.

Higher-order terms can be obtained and determined with the help of Mathematica software up to the desired accuracy. In figure B1, we report the relative error on the MF value of the single-particle partition function $z(\beta, \mu)$ versus the approximation order k for some values of w (both for positive and negative temperatures).

As expected, the very high accuracy for small w values degrades when w becomes of order 1. A second feature is that the accuracy of the expansion initially increases with k up to some k^* when it starts degrading. This is a clear indication of the asymptotic nature of the series expansion in powers of w. Finally, the overlap of data obtained for the same w but a different sign of β indicates that the sign is irrelevant.

Appendix C. $T = 0$ limit

In the low-temperature limit, we can approximate the expressions for the partition function z, a, q, and h by using the leading term of the modified Bessel functions $I_{0,1}$ for large argument v

$$I_{0,1}(v) \simeq \frac{\mathrm{e}^{v}}{\sqrt{2\pi v}}. \tag{C.1}$$

By substituting equation (C.1) into equation (11), z can be rewritten as

$$z \simeq \int_0^\infty \mathrm{d}c \sqrt{\pi} \frac{\mathrm{e}^{\beta A(c)}}{\sqrt{\beta q} c^{1/4}}, \tag{C.2}$$

where

$$A(c) = -c^2 + \mu c + 2q\sqrt{c}. \tag{C.3}$$

We can now use the saddle-point method to approximate z as

$$z \simeq \sqrt{\pi} \frac{\mathrm{e}^{\beta A\left(c^*\right)}}{\sqrt{\beta q} c^{*1/4}}, \tag{C.4}$$

where c^* is the mass value that maximizes $A(c)$ and therefore satisfies the relation

$$\left.\frac{\partial A(c)}{\partial c}\right|_{c=c^*} = 2c^* - \frac{q}{\sqrt{c^*}} - \mu = 0. \tag{C.5}$$

We can also derive the expression for q in the low-temperature limit,

$$q \simeq \frac{1}{z} \int_0^\infty \mathrm{d}c \sqrt{c} \sqrt{\pi} \frac{\mathrm{e}^{\beta A(c)}}{\sqrt{\beta q} c^{1/4}} \simeq \sqrt{c^*} \frac{\sqrt{\pi}}{z} \frac{\mathrm{e}^{\beta A\left(c^*\right)}}{\sqrt{\beta q} c^{*1/4}} = \sqrt{c^*}, \tag{C.6}$$

and similarly for the expressions for a and h

$$a \simeq \frac{1}{z} \int_0^\infty \mathrm{d}c\, c \sqrt{\pi} \frac{\mathrm{e}^{\beta A(c)}}{\sqrt{\beta q} c^{1/4}} \simeq c^*, \tag{C.7}$$

$$\begin{aligned} h &\simeq \frac{1}{z} \int_0^\infty \mathrm{d}c \left(c^2 - 2q\sqrt{c}\right) \sqrt{\pi} \frac{\mathrm{e}^{\beta A(c)}}{\sqrt{\beta q} c^{1/4}} \\ &\simeq c^{*2} - 2\sqrt{c^*} q \simeq a^2 - 2a. \end{aligned} \tag{C.8}$$

Analogously, we find $h_{\mathrm{nl}} \simeq a^2$ and $h_{\mathrm{int}} \simeq -2a$.

If we substitute equations (C.6) and (C.7) in equation (C.5), we obtain

$$c^* = a = \frac{\mu + 1}{2}, \tag{C.9}$$

that is, a relation between a and the chemical potential μ for the MF model.

For the complete DNLS model, using the saddle-point method we obtain a different relation between a and μ in the low-temperature limit

$$\mu_{\rm DNLS}^{(T=0)} = 2\,(a-1) \tag{C.10}$$

and if we replace a with equation (C.9), we obtain a relationship between the chemical potentials in the two models

$$\mu_{\rm MF}^{(T=0)} = \mu_{\rm DNLS}^{(T=0)} + 1. \tag{C.11}$$

Appendix D. Ratio of energy differences *R*

If we combine equations (B.14)–(B.17) retaining all terms up to the order w, we find

$$\Delta h_{\rm nl} \equiv h_{\rm c} - h_{\rm nl} = \frac{4w}{m^2} \tag{D.1}$$

$$\Delta h \equiv h_{\rm c} - h = \frac{4w}{m^2} + \frac{\pi\, w}{2}, \tag{D.2}$$

so that

$$R \equiv \frac{\Delta h_{\rm nl}}{\Delta h} = \frac{4}{4 + \pi\, m^2/2} \tag{D.3}$$

which tends to $8a^2/\pi$ for small a and to 1 for large a.

References

[1] Kevrekidis P G 2009 *The Discrete Nonlinear Schrödinger Equation: Mathematical Analysis, Numerical Computations and Physical Perspectives* vol 232 (Springer Science & Business Media)
[2] Mithun T, Kati Y, Danieli C and Flach S 2018 *Phys. Rev. Lett.* **120** 184101
[3] Arezzo C, Balducci F, Piergallini R, Scardicchio A and Vanoni C 2022 *J. Stat. Phys.* **186** 1–23
[4] Giachello M, Iubini S, Livi R and Gradenigo G 2025 *J. Stat. Mech.* **2025** 113101
[5] Kabat E, Mohapatra S, Kevrekidis P and Kottos T 2026 arXiv:2602.13161
[6] Baldovin M, Iubini S, Livi R and Vulpiani A 2021 *Phys. Rep.* **923** 1–50
[7] Tsironis G 2025 The discrete nonlinear Schrödinger equation: from biomolecules to nonlinear optics to Bose-Einstein condensates *Artificial Intelligence and Complex Dynamical Systems* (Springer) pp 97–120
[8] Flach S and Willis C R 1998 *Phys. Rep.* **295** 181–264
[9] Iubini S, Franzosi R, Livi R, Oppo G L and Politi A 2013 *New J. Phys.* **15** 023032
[10] Rumpf B 2009 *Physica D* **238** 2067–77
[11] Ebrahimi M, Drossel B and Just W 2025 *Physica D* **482** 134905
[12] Iubini S and Politi A 2025 *Phys. Rev. Lett.* **134** 097102
[13] Iubini S, Chirondojan L, Oppo G L, Politi A and Politi P 2019 *Phys. Rev. Lett.* **122** 084102
[14] Politi A, Politi P and Iubini S 2022 *J. Stat. Mech.* **2022** 043206
[15] Machlup S 1975 *Am. J. Phys.* **43** 991–5
[16] Rasmussen K Ø, Cretegny T, Kevrekidis P G and Grønbech-Jensen N 2000 *Phys. Rev. Lett.* **84** 3740
[17] Iubini S, Politi A and Politi P 2014 *J. Stat. Phys.* **154** 1057–73
[18] Gotti G, Iubini S and Politi P 2021 *Phys. Rev. E* **103** 052133
[19] Szavits-Nossan J, Evans M R and Majumdar S N 2014 *Phys. Rev. Lett.* **112** 020602

J. Stat. Mech. (2026) 053201

[20] Giusfredi M, Iubini S and Politi P 2024 *J. Stat. Phys.* **191** 119
[21] Giusfredi M, Iubini S, Politi A and Politi P 2025 *J. Stat. Mech.* **2025** 053203
[22] Gradenigo G, Iubini S, Livi R and Majumdar S N 2021 *J. Stat. Mech.* **2021** 023201
[23] Gradenigo G, Iubini S, Livi R and Majumdar S N 2021 *Eur. Phys. J. E* **44** 1–6
[24] Evans M R and Hanney T 2005 *J. Phys. A: Math. Gen.* **38** R195
[25] Iubini S, Lepri S and Politi A 2012 *Phys. Rev. E* **86** 011108
[26] Andrews G E, Askey R and Roy R 1999 Special functions *Encyclopedia of Mathematics and its Applications* (Cambridge University Press)